Interface-state properties for strained-layer Ni adsorbed on Ru(0001)

J. E. Houston, J. M. White,* and P. J. Feibelman
Sandia National Laboratory, Albuquerque, New Mexico 87185

D. R. Hamann
AT&T Bell Laboratories, Murray Hill, New Jersey 07974
(Received 29 July 1988)

Studies of ultrathin layers of Ni on Ru(0001) by He I photoemission and theoretical calculations reveal the existence of surface and interface states resulting from the Ni($3d$)-Ru($4d$) interaction. Pure Ni surface states are found centered at a binding energy of about -1.4 eV. Split about this position are two pairs of Ni-Ru states of different symmetry character. The highest lying of these states is identified as an interface state of mostly Ni character and $d\sigma$ symmetry, while the most tightly bound ones are identified as mostly Ru in character and of $d\sigma$ symmetry. The splitting between these interface states is 3.1 eV, reflecting a combination of the d-band offset of Ni relative to Ru and the level repulsion engendered by the Ni-Ru interaction. A similar combination of states with mixed $d\pi$-$d\delta$ symmetry is found having a splitting of about 2.7 eV. Analogous states are found for the Cu/Ru(0001) bimetallic system. The two systems differ principally due to the relative positions of the d states for Cu (deeper) compared to Ni.

I. INTRODUCTION

Interface states have been identified and their properties explored both experimentally and theoretically for films of Cu on the Ru(0001) surface.[1,2] During deposition of the first monolayer (ML), Cu grows in 2D islands with the atoms arranged pseudomorphically to the Ru substrate structure.[3] Since Cu is a smaller atom than Ru, this structure places the Cu films under approximately a 6% tensile strain relative to bulk Cu.

Angle-resolved photoemission (ARUPS) studies and theoretical calculations revealed the existence of two pairs of states with electron densities highly localized on the Cu and the outermost Ru layers (interface states) in a region of the surface Brillouin zone (SBZ) near the $\bar{K}$ point.[1,2] One pair had binding energies centered at about -1.5 eV and the other at approximately -3.6 eV. The pairs were split in energy by about 0.1 eV. These interfacial levels were produced by a strong interaction between Cu($3d$) and Ru($4d$) states and the two pairs had $d\sigma$ and mixed $d\pi$ and $d\delta$ symmetries with respect to the surface normal at a Cu-atom site. A third pair of states (localized on Cu) was identified having binding energies centered at about -2.6 eV, an energy separation of approximately 40 meV, and mixed $d\pi$ and $d\delta$ symmetries.[1,2]

The Cu/Ru interface states provide a unique diagnostic tool in studies of interactions of the bimetallic surface with adsorbate species.[2] The facts that the interface states have d character, are more than 0.5 eV closer to the Fermi level than the d states of bulk Cu, and have favorable symmetries were used to investigate the origin of the observation that CO has a binding energy to the bimetallic surface which is intermediate between its values for bulk Cu and Ru.[3] From these studies it was concluded that (1) CO bonding to bulk Cu and to the Cu/Ru bimetallic surface involves a negligible direct interaction between CO orbitals and metallic d states and (2) the enhanced bonding to the bimetallic surface results from an increased s-state polarization of the Cu surface due to the presence of the more electronegative Ru substrate.[2]

In order to understand the origins of the interesting chemical and catalytic behavior of bimetallic surfaces in general,[4] and the Cu/Ru system in particular,[5] it is important to characterize their structural and electronic properties. A systematic approach should include varying the bimetallic combination, and we have begun this work by studying the structure of Cu's neighbor Ni on the Ru(0001) surface.[6] In the present paper, we extend the study of the Ni/Ru system to its electronic properties. We report the results of ARUPS measurements together with surface linearized augmented-plane-wave (LAPW) calculations to establish the existence and probe the properties of surface and interface states for this bimetallic system.

II. EXPERIMENTAL AND THEORETICAL TECHNIQUES

A. Experimental

The Ru(0001) surface was cleaned by exposure to approximately 1000 L [1 Langmuir (L)$=10^{-6}$ Torr sec] of O_2 through a microchannel-plate doser at a sample temperature of 1450 K followed by a vacuum bake at 1550 K for 300 sec. The cleanliness was verified by Auger spectroscopy. For the principal contaminant C, whose Auger structure is obscured by that of Ru, we used the accepted scheme of measuring the negative-to-positive peak ratios in $dN(E)/dE$ Auger data for the Ru structure near 270 eV.[7,8] Ni deposition was accomplished by evaporation onto the Ru surface at room temperature from a resis-

tively heated W filament wrapped with high-purity Ni wire. The bimetallic surfaces were subsequently annealed to near 350 K which, according to low-energy electron diffraction (LEED) measurements,[6] assured a well-ordered overlayer. The Ni source was outgassed thoroughly prior to deposition and no contamination could be detected as a result of the sample exposure. The deposition was controlled by varying the voltage across the W filament and the rate was monitored with a line-of-sight mass spectrometer. The Ni coverages were accurately established by temperature-programmed desorption (TPD).[6]

ARUPS energy distribution curves were measured using a Vacuum Generators ADES 400 system with an unpolarized He-discharge lamp. The energy resolution of the electron analyzer was approximately 0.1 eV and the angular acceptance was about $\pm 1°$. He I photons ($h\nu = 21.2$ eV) impinged on the sample surface along the surface normal and photoelectrons were detected at various polar angles corresponding to $k_{\parallel}$ values along the $\bar{\Gamma}$-$\bar{K}$ line in the SBZ. The azimuthal detection angle to achieve this SBZ orientation was established by LEED.

B. Theoretical

Our surface electronic-structure calculations utilized the LAPW method[9] modeling the 1-ML-Ni/Ru adsorption system as a five-layer Ru(0001) slab with a pseudomorphic Ni adlayer on either side. The Ru atoms of the slab were placed at bulk Ru relative positions. In the absence of actual structural measurements for the pseudomorphic Ni overlayer, Ni atoms were placed in plausible adsorption sites, namely threefold hollows[10] with the Ni—Ru bond length chosen to equal the average of the Ru-Ru and Ni-Ni nearest-neighbor distances in the respective bulk metals. The calculations were semirelativistic,[9] and represented the effects of exchange and correlation with the local density-functional exchange-correlation potential[11] based on the Wigner interpolation formula.[12] Further details of the calculational method can be found in Refs. 9 and 13.

In the absence of experimental information to the contrary, the Ni adlayers were assumed to be paramagnetic. Calculations for other bimetallic systems suggest enhanced magnetism in magnetic monolayers on nonmagnetic substrates.[14] Including such a phenomenon here would likely result in a doubling of the number of Ni-induced UPS features and shifts of tenths of eV in their positions.[15]

In order to see more clearly where the surface and interface states lie relative to the bulk Ru bands, we computed the surface-projected, bulk Ru band structure as follows. A self-consistent electronic-structure calculation was carried out for bulk Ru. The one-electron energy levels were then evaluated for a set of $\mathbf{k}$ vectors of the form

$$\mathbf{k} = (k_{\parallel}, k_{\perp}) ,$$

where $k_{\parallel}$ lies along the line $\bar{\Gamma}$-$\bar{K}$ in the SBZ and $k_{\perp} = 2\pi n / Nc$ ($n = 0, 1, 2, \ldots, N$). Here, c is the unit-vector length along the Ru c axis (equal to 4.28 Å). The surface-projected bulk band structure was constructed as a plot of the energy eigenvalues for every $k_{\perp}$ corresponding to a set of discrete values of $k_{\parallel}$ ranging from $\bar{\Gamma}$ to $\bar{K}$. This plot not only shows the dispersion of bulk bands with respect to the SBZ, but also enables one to see the *density-of-states* (DOS) for the projected bulk bands across the SBZ. N was chosen to be 38 in the expression for $k_{\perp}$ above in order to clearly convey the surface projected DOS.

III. RESULTS

Figure 1 shows He I ARUPS energy-distribution curves (EDC's) as a function of detection angle over the binding-energy range from the Fermi energy (binding energy of 0) to about -7.0 eV for both clean Ru(0001) [Fig. 1(a)] and for 1 ML Ni adsorbed on the Ru(0001) surface [Fig. 1(b)]. Also shown in Fig. 1 are the values of $k_{\parallel}$ for photoemission from the Fermi level along the $\bar{\Gamma}$-$\bar{K}$ symmetry line corresponding to each detection angle. Since the photoemission cross section for He I radiation is approximately the same for Ni($3d$) relative to Ru($4d$) states and for Ni($4s$) in relation to Ru($5s$) states,[16] relative changes in the data of Fig. 1 result only when the addition of Ni causes the creation or movement of states with sufficient contrast.

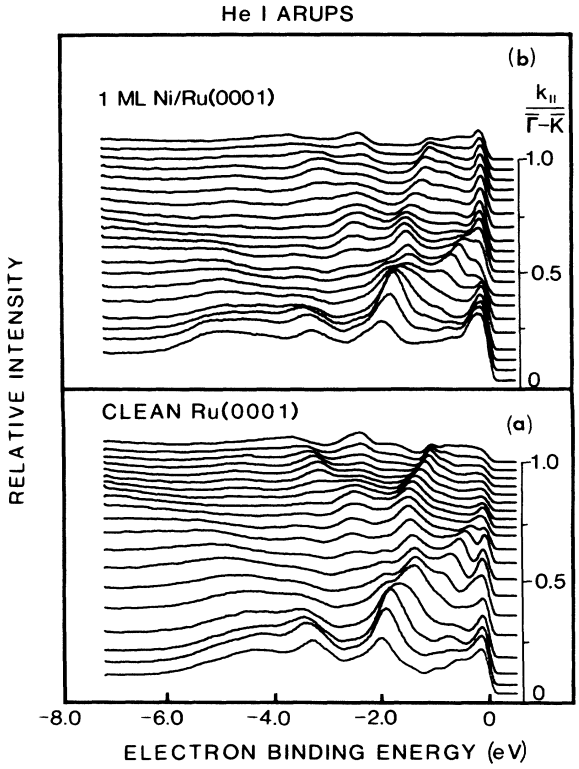

FIG. 1. He I ARUPS results for (a) the clean Ru(0001) surface and (b) for the 1-ML-Ni/Ru(0001) bimetallic surface. In each case a series of energy distribution curves is presented as a function of relative SBZ position along the $\bar{\Gamma}$-$\bar{K}$ symmetry line. The relative zone positions shown on the abscissa (given as the ratio of the $k_{\parallel}$ value to the total $k_{\parallel}$ difference between the $\bar{K}$ and $\bar{\Gamma}$ points) refer to electrons emitted from the Fermi level.

Comparing the ARUPS EDC behavior of Figs. 1(a) and 1(b) indicates that, for the most part, the adsoprtion of 1 ML of Ni causes only subtle changes of the clean Ru spectrum. The most prominent change is in the region near $\bar{K}$, an increase in emission at the Fermi energy. From this result, it is obvious that the Ni overlayer gives rise to a rather sharp band of states near the Fermi level in the region of the SBZ near $\bar{K}$. These states are readily observed not only because they are distributed over a small portion of the SBZ but also because they lie in a region of low intensity in the clean Ru spectra. Further insight into their properties can be obtained by studying their behavior with respect to Ni coverage.

Figure 2(a) shows a series of ARUPS EDC's taken at the $\bar{K}$ point in the SBZ with increasing Ni coverage. The addition of Ni causes an increase in intensity at the Fermi level which saturates at 1 ML. Adding more Ni gives rise to intensity in the region below the original peak. As the coverage increases structures form which approach those of clean Ni(111), shown in Fig. 2(b).

A more detailed picture of the effect of 1 ML Ni on the Ru surface can be obtained by subtracting the clean Ru spectrum from the 1-ML-Ni/Ru spectrum. This difference curve (Fig. 3) reveals several features in addition to the near-Fermi-level structure. Two poorly resolved features are found at binding energies of approximately -0.65 and -0.88 eV, along with peaks at about -2.2 and -3.0 eV. A weak shoulder is also detected at a binding energy of approximately -1.4 eV. In addition, close inspection of the near-Fermi-level peaks reveals that the breadth of its low binding-energy edge is the result of instrumental broadening, indicating that this feature straddles the Fermi edge.

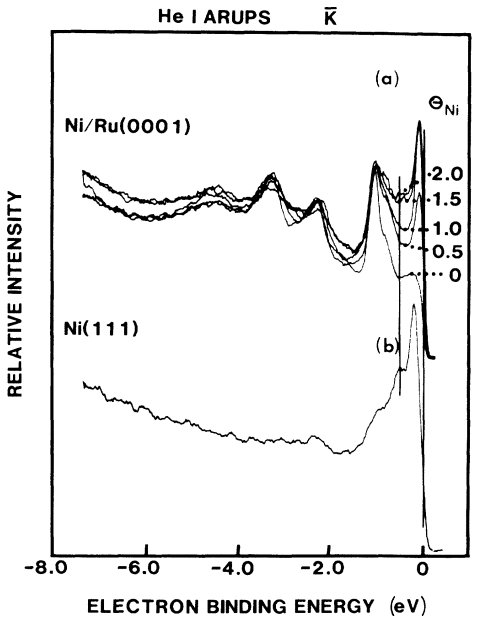

FIG. 2. He I ARUPS results for the Ni/Ru(0001) bimetallic surface as a function of Ni coverage taken at the $\bar{K}$ point in the SBZ. The Ni overlayers were deposited at 100 K and annealed to 700 K. For comparison photoemission from a clean bulk Ni(111) surface is also shown.

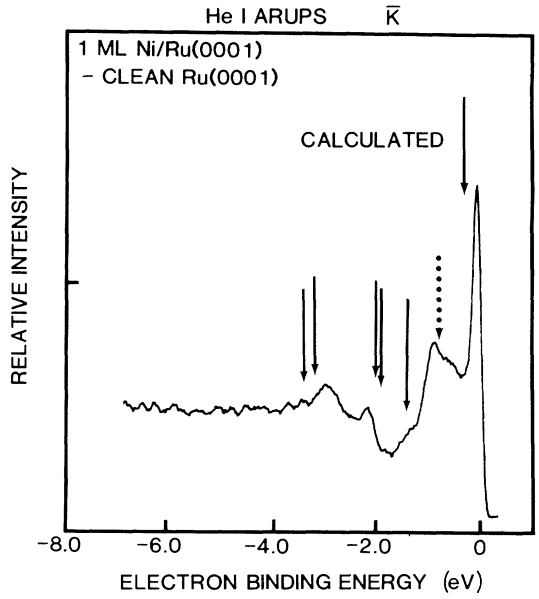

FIG. 3. He I ARUPS results for the 1-ML-Ni/Ru(0001) bimetallic surface taken at the $\bar{K}$ point in the SBZ and corrected for the clean substrate contribution by spectral subtraction. The arrows mark the positions of surface and/or interface states calculated theoretically.

Surface and interface states found in the LAPW calculations, at the $\bar{K}$ point, are indicated by the vertical arrows in Fig. 3. We identify these surface and interface states as those whose wave functions are strongly localized at the Ni overlayer, or are shared between the Ni overlayer and outermost Ru layer, while having little contribution at the interior "bulk" Ru layers. The set of states highlighted with solid arrows in Fig. 3 are those which have more than 80% of their electron density contained in the Ni and outermost Ru layers relative to that contained in all "bulk" layers. The surface or shared interface character of each such state is determined by the relative weighting of the charge density between the Ni overlayer and the Ru outer layer. The results concerning the detailed nature of these states at the $\bar{K}$ point are given in Table I, which indicates surface and interface character as well as symmetry properties. Each of the states listed in Table I appears in the calculations as a pair of levels split in energy by a few hundredths of an eV or less. This splitting is indicative of the magnitude of the interference effects resulting from the use of a slab model of only a few layers in thickness. In Table I, the value listed represents the average binding energy for these split states.

The comparison between experiment and theory in Fig. 3 shows that all of the calculated states have corresponding features in the experimental spectrum and the agreement is within a few tenths of an eV. The feature with its peak appearing near -1.0 eV is not found in the calculations with surface and/or interface localization sufficient to meet the criterion of Table I. However, states with an average binding energy of -0.8 eV are predicted which can be described as surface and/or interface resonances

TABLE I. Surface and interface character, as well as symmetry properties, of states at the $\bar{K}$ point that have more than 80% of their electron density contained in the Ni and outermost Ru layers relative to that contained in all "bulk" layers.

Binding[a] energy (eV)	Surface and/or interface[b] character (%) Ni+Ru$^{(o)}$	Ni	Ru$^{(o)}$	Ni-site symmetry[c] character (%) $d\sigma$	$d\pi$	$d\delta$[d]
−0.28	100	80	20	100		
−1.37	100	100			59	41
−1.46	90	84	6		47	53
−1.98	79	71	8		44	50
−3.26	92	30	62		62	38
−3.41	98	26	72	69[e]		

[a]Binding energies are referenced to E_F and are rounded to three significant figures.
[b]Muffin-tin electron densities for both Ni and outer Ru-layer muffin tins (Ru$^{(o)}$) have been normalized to the sum of contributions from all layer muffin tins.
[c]These numbers were obtained by integrating $|\psi_{lm}|^2$ in each muffin tin and expressing the result as a percentage of $\sum_{l,m}\int|\psi_{lm}|^2$ for all muffin tins.
[d]$d\sigma$ refers to orbitals with $d_{3z^2-r^2}$ symmetry characterization while $d\pi$ refers to d_{xz} and d_{yz} and $d\delta$ refers to d_{xy} and $d_{x^2-y^2}$.
[e]The remaining portion of the charge density for this state is of $p\pi$ and s symmetry character.

because of their weak localization. It seems reasonable to associate the feature near −1.0 eV with this apparent surface resonance, which is illustrated in Fig. 3 by the dotted line. According to Table I, the principal feature near the Fermi energy is 100% localized on the Ni and outer Ru layers with 80% of the electron density on the Ni overlayer (i.e., it is essentially a Ni surface state). These calculated states have $d\sigma$ symmetry ($d_{3z^2-r^2}$) with respect to the surface normal at the Ni sites.

From Fig. 1 it is clear that the additional intensity near the Fermi level produced by the Ni overlayer extends to the interior of the SBZ from $\bar{K}$ towards $\bar{\Gamma}$. The calculations permit a careful analysis of the SBZ behavior for all of the states indicated in Fig. 3 by placing them onto the surface-projected band structure for Ru(0001) to see their relationship to the Ru bulk bands. Before proceeding, however, we first show the relationship between the calculated surface-projected band structure and the clean-surface EDC behavior shown in Fig. 1(a). This comparison is shown in Fig. 4.

In Fig. 4, the array of open circles represents the calculated (0001) surface-projected bulk band structure for Ru obtained as described earlier. Regions of this plot with high density of states, i.e., with a high density of circles, occur either where the projected bands are narrow with respect to $k_\perp$ or where these bands have small slopes with respect to variations of $k_\perp$. An example of the former behavior can be seen at the bottom of the lowest band near the $\bar{\Gamma}$ point (which is principally of 5s character) while the latter behavior is represented by the center band near the $\bar{K}$ point (at about −3.0 eV, which is largely of 4d character).

It should be recalled that probing the $k_\parallel$ behavior of band states with photoemission using fixed-energy photons involves the detection of photoelectrons at various angles of emission and, thus, probes variations with both $k_\parallel$ and $k_\perp$.[17] In the present case, and under the assumption of free-electron final-state bands with a 14-eV inner potential,[18] varying the detection angle over the range from $\bar{\Gamma}$ to $\bar{K}$, corresponding to the data shown in Fig. 1(a), implies a variation of $k_\perp$ approximately between Γ and A in the fourth bulk zone.

Schematically, assuming vertical transitions, bulk photoemission intensity occurs when valence electrons at $\mathbf{k}=(k_\perp,k_\parallel)$ are excited from initial states, like those illustrated by the circles in Fig. 4, into conduction-band final states at $\mathbf{k}$ which are $\hbar\omega$ higher in energy. For a fixed photon energy, the intensity is therefore proportional to

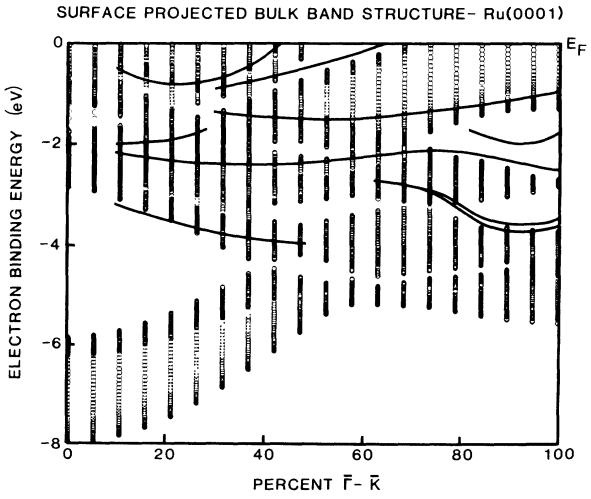

FIG. 4. A comparison between the surface-projected density of states calculated for the clean Ru(0001) surface (circles) and the He I ARUPS results from Fig. 1(a) (solid lines). Only those features in Fig. 1(a) which have sufficient contrast to be readily followed are shown.

the initial-state DOS at **k** modulated by the final-state DOS at **k**. In practice, the modulation function tends to be rather broad because of the effect of the surface sensitivity of the technique, i.e., the short mean free path of the final-state electron, and because of the limited lifetimes of the photoelectrons within the solid (broadening which increases with the photoelectron energy[19]). The contrast of photoemission structures is also diminished as a result of the low-energy tail that accompanies these structures due to the effect of losses suffered by the photoelectrons in their transport to the surface. When, as a result of these factors, the final-state modulation is weak, photoemission data will follow regions of the projected valence-band structure which are narrow in energy and of high state density. This makes the particular scheme we use for visualizing the projected DOS a valuable one.

In Fig. 4, the solid lines indicate the $k_{\parallel}$ behavior of those features in the EDC's of Fig. 1(a) which have enough contrast to be specifically identified. Although there appears to be a consistent energy shift of about 0.2 eV between the experimental and calculated binding energies (the calculated values being larger), the general trend is that the experimental data (with a few exceptions) tend to follow the paths of high projected density of states. The bands below about -4.0 eV have insufficient contrast to be delineated in the experimental data.

The exceptions are several experimentally observed features which reside in gaps of the projected states. These include a feature at a binding energy of about -3.0 eV near the 30% position in the zone, a feature crossing the Fermi level at about 65% and two features near $\bar{K}$ at binding energies of about -2.0 and -3.5 eV, respectively. Since these features appear in gaps in the projected bulk band structure, we interpret them as surface states or resonances whose wave functions die off as one moves into the bulk. The gap state near the $\bar{K}$ point at a binding energy of about -2.0 eV has been identified in earlier calculations.[20] A second state, predicted in this region, cannot be identified in the data.

Surface states, or resonances, by their nature have negligible $k_{\perp}$ dispersion and often appear with high contrast in photoemission data. They become less surface localized as they approach a band edge, assuming the symmetry of the band allows mixing, and their contrast rapidly diminishes. Qualitatively, this behavior is characteristic of all the surface-state features discussed earlier. From Fig. 4 these include (1) the feature at about -3.0 eV near $\bar{\Gamma}$, (2) the structure crossing the Fermi level at about 65% $\bar{\Gamma}$-$\bar{K}$, and (3) all four of the gap states near $\bar{K}$. In each case as the state approaches the edge of the projected bulk bands, its intensity dramatically decreases. Although the features in Fig. 4 associated with the bulk bands tend to follow regions of high density of states in the projected-states calculation, an analysis of the intensity of these features with respect to zone position is considerably more complex and is beyond the scope of the present paper. The value of presenting photoemission data relative to the surface-projected bulk DOS, as in Fig. 4, is that it allows one to determine regions where final-state band dispersion has an appreciable effect and to evaluate photoemission results with respect to their band structure or density-of-states sensitivity.[19]

In Fig. 5 we show the situation for 1-ML-Ni/Ru(0001) corresponding to the clean Ru comparison of Fig. 4. Only those features are followed (solid lines) which can be clearly identified in difference curves (similar to Fig. 3) as due to the addition of Ni. The behavior of the calculated states is shown by dotted lines in Fig. 5. For the experimental data, the comparison is continued away from $\bar{K}$ toward $\bar{\Gamma}$ only to the extent that the states can be clearly identified (enough contrast). For the calculations, only those states were chosen for which the surface or interface character exceeded 80%.

Two distinct types of surface or interface states can be identified in the comparison of Fig. 5. First, a group of states residing in gaps in the surface-projected bulk band structure. One of these crosses the Fermi level at about the 62% point while three others lie in gaps near the $\bar{K}$ point in the SBZ and have binding energies of about -1.5, -2.0, and -3.3 eV. Experiment and theory are in excellent agreement for the first of these states and for the state at about -1.5 eV. The remaining two have binding-energy predictions which differ by several tenths of an eV. According to the calculations, the states near -1.5 and -2.0 eV are virtually pure-Ni surface states with mixed $d\pi$ and $d\delta$ symmetry character (Table I). The state near -3.3 eV is more interfacial in nature but with a strong Ru surface-state character having a mixed $d\pi$ and $d\delta$ symmetry character. The state crossing the Fermi energy near the center of the $\bar{\Gamma}$-$\bar{K}$ line has about 91% surface and/or interface localization with 86% attributable to Ni surface states. In this case the symmetry character is almost pure $d\delta$.

The other level compared in Fig. 5 lies within a broad

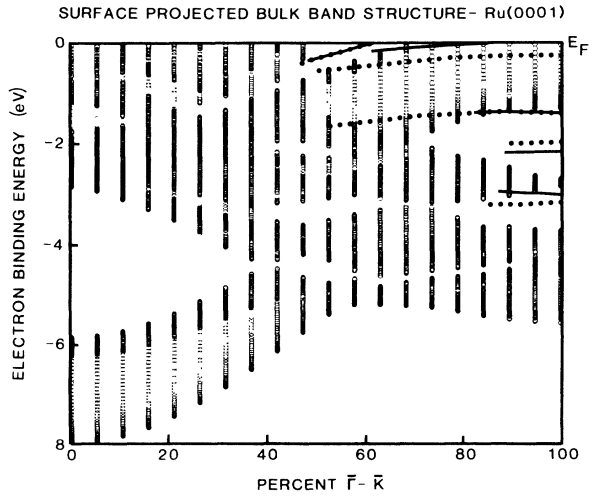

FIG. 5. A comparison between the He I ARUPS results for the surface and/or interface features from difference curves similar to that of Fig. 3 (solid lines) and the calculated behavior for which the surface and/or interface character exceeded 80% (dotted curves). Only those experimental features which have sufficient contrast to be readily followed are shown. This comparison is plotted on surface-projected bulk band structure of Fig. 4 (circles).

band of states which is split by the Fermi level at $\bar{K}$ and which extends to binding energies of almost -1.5 eV at this point. The most intense contribution in the experimental data is from this state straddling the Fermi level near $\bar{K}$. According to the calculations, this state is predicted in Fig. 5 to lie below the Fermi level at about -0.28 eV. The calculation shows that this state is strongly interface localized with considerable weighting towards the Ni overlayer and is of pure $d\sigma$ symmetry.

It is conceivable that the discrepancies between theory and experiment are at least in part associated with magnetism of the Ni overlayers. An exchange splitting of ~ 0.3 eV would be difficult to resolve in the data of Fig. 2. The worst disagreement is for the observed state at E_F. However, the fact that the corresponding theoretical state lies deeper suggests that the discrepancy arises from using the local density-functional approximation. Magnetism would tend to make the experimentally observed (majority spin) state lie deeper.

IV. DISCUSSION

In order to establish a better understanding of the Ni/Ru results summarized in Fig. 5 and Table I, it is instructive to make a direct comparison with similar results obtained earlier for the Cu/Ru system.[1,2] Figure 6 shows this comparison from the calculated results at the $\bar{K}$ point in the SBZ with the energy position of the states for the two systems plotted vertically. Also noted in Fig. 6 are the symmetry properties for the various states as well as their relative surface and/or interfacial localization character.

As described earlier for the Cu/Ru system,[1,2] the results summarized in Fig. 6 appear relatively simple. A set of pure-Cu states (i.e., Cu surface states) resides at a binding energy of approximately -2.6 eV just above the narrow band of projected bulk states centered near -2.8 eV. These states have mixed $d\pi$ and $d\delta$ symmetry and the highest binding-energy component, which is closest to the surface-projected bulk band, is slightly less localized to the Cu overlayer. In addition, two sets of states are found above and below the Cu surface states. These states have appreciable interfacial character and represent the bonding-antibonding components of states with a strong Cu($3d$)-Ru($4d$) bonding interaction.[1,2]

For the Ni-Ru system, the main difference can be attributed to the weaker binding of the Ni d electrons relative to those of Cu. This accounts immediately for the fact that the pure-Ni surface states lie near -1.4 eV rather than at -2.6 eV for the pure-Cu states in Cu/Ru. It also explains why the splitting of the $d\sigma$ Ni-Ru interface states is 3.1 eV, larger than the value of 2.3 eV found for Cu/Ru. In the present case, the energy mismatch of the Ni and Ru d states adds to the level repulsion associated with hybridization to produce the larger splitting. For completeness, we also show as the dotted line in Fig. 6 the position of the surface resonance discussed earlier with reference to Fig. 3.

The substantial shift of the Ni d levels up away from resonance with the Ru d bands also accounts for the diminished mixing of Ni and Ru character in the interface states. The weak Ni-Ru hybridization is manifest in the fact that the high-lying interface states are mostly Ni-like while the low-lying states are mostly Ru-like. This contrast with the Cu-Ru case where the Cu and Ru character of the interface states was more nearly equal. The weakness of the Ni-Ru hybridization is also clear in the fact that the upper Ni-Ru interface states are quite strongly surface localized despite their overlapping bulk Ru bands.

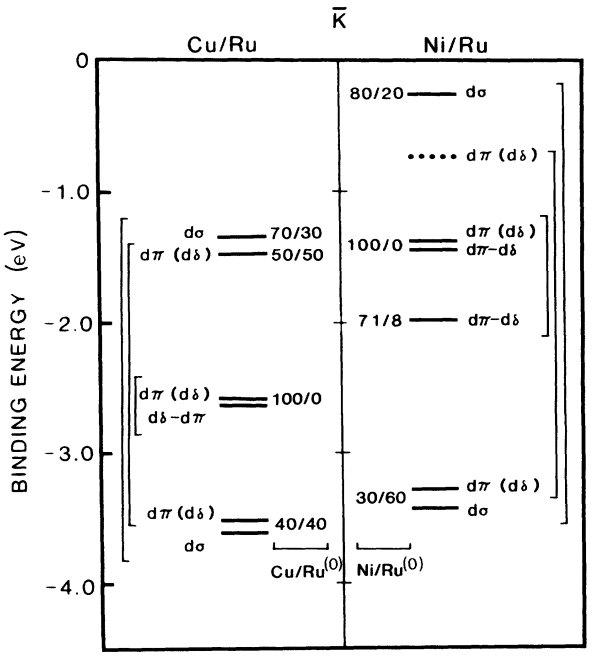

FIG. 6. A summary comparison between the calculated surface and interface states found for the Cu/Ru(0001) and Ni/Ru(0001) bimetallic systems. The binding energies are plotted vertically and the symmetry character and relative surface and/or interface localization is schematically indicated for each state. Where mixed symmetry is found, the relative weighting of the components is indicated by their order [i.e., $d\sigma(d\delta)$ implies $d\sigma$ larger than $d\delta$ while $d\sigma$-$d\delta$ indicates approximately equal weighting]. The relative surface and/or interface localization, e.g., 60/30, indicates that the charge densities for these states are found to be 60% on the Ni overlayer, 30% on the outermost Ru layer, and 10% distributed within the Ru bulk layers. The dotted line indicates the surface resonance mentioned in the text in reference to Fig. 3.

V. SUMMARY AND CONCLUSIONS

A set of surface and interface states has been identified and analyzed for the Ni/Ru(0001) bimetallic surface by angle-resolved photoemission and theoretical calculations. These states consist of pure-Ni surface states along with a series of interface states resulting from a relatively weak Ni($3d$)-Ru($4d$) hybridization. Over a significant portion of the surface Brillouin zone, the high-lying components of the interface states give rise to a considerable

increase in the density of d states near the Fermi level compared to that found for either bulk Ni(111) or Ru(0001). These states have either $d\sigma$ or mixed $d\pi$ and $d\delta$ symmetry.

Good correspondence is found between the electronic properties for the Ni/Ru and Cu/Ru bimetallic systems[1,2] with the differences resulting principally from the d-level positions in Ni versus Cu. In the Cu/Ru system, the unique properties of these surface and interface states have been used to diagnose the details of the bonding interaction of the bimetallic surface with small molecules[2] and similar work involving the Ni/Ru system offers the promise of providing valuable information concerning the contrast in chemical properties between these two catalytically interesting materials.

ACKNOWLEDGMENTS

The authors would like to express their gratitude to P. J. Berlowitz and D. W. Goodman for stimulating discussions and to T. E. Madey for the kind loan of his Ru(0001) crystal. The portion of the work done at Sandia National Laboratory was sponsored by the U.S. Department of Energy under Contract No. DE-AC04-76DP00789. We also acknowledge the partial support of this work by the Department of Energy, Office of Basic Energy Sciences, Division of Materials Sciences. J. M. White received support from the Sandia National Laboratories Summer Visiting Faculty Program.

---

*Permanent address: Chemistry Department, University of Texas, Austin, TX 78712.

[1]J. E. Houston, C. H. F. Peden, P. J. Feibelman, and D. R. Hamann, Phys. Rev. Lett. **56**, 375 (1986).

[2]J. E. Houston, C. H. F. Peden, P. J. Feibelman, and D. R. Hamann, Surf. Sci. **192**, 457 (1987).

[3]J. E. Houston, C. H. F. Peden, D. S. Blair, and D. W. Goodman, Surf. Sci. **167**, 427 (1986).

[4]See, for example, J. H. Sinfelt, Acc. Chem. Res. **10**, 15 (1977).

[5]C. H. F. Peden and D. W. Goodman, J. Catal. **100**, 520 (1986); **104**, 347 (1987).

[6]P. J. Berlowitz, J. E. Houston, J. M. White, and D. W. Goodman (unpublished).

[7]P. D. Reed, C. M. Comrie, and R. M. Lambert, Surf. Sci. **59**, 33 (1976).

[8]T. W. Orent and R. S. Hansen, Surf. Sci. **67**, 325 (1977).

[9]D. R. Hamann, L. Mattheiss, and H. S. Greenside, Phys. Rev. B **24**, 6151 (1981).

[10]Both hcp sites (defined as threefold positions which have a Ru atom directly below) and fcc sites (defined as threefold sites with no Ru in the second underlying layer) were probed in the calculations.

[11]*Theory of the Inhomogeneous Electron Gas*, edited by S. Lundquist and N. H. March (Plenum, New York, 1983).

[12]E. Wigner, Phys. Rev. **46**, 1002 (1934).

[13]L. Mattheiss and D. R. Hamann, Phys. Rev. B **33**, 823 (1986).

[14]C. L. Fu, A. J. Freeman, and T. Oguchi, Phys. Rev. Lett. **54**, 2700 (1985).

[15]See, O. Jepsen, J. Madsen, and O. K. Andersen, Phys. Rev. B **26**, 2790 (1982), and references therein.

[16]S. M. Goldberg, C. S. Fadley, and S. Kono, J. Electron. Spectrosc. **21**, 285 (1981).

[17]F. J. Himpsel, Appl. Opt. **19**, 3964 (1980).

[18]M. Lindroos, P. Hofmann, and D. Menzel, Phys. Rev. B **33**, 6798 (1986); this value is in good agreement with the 13.6 eV figure which can be obtained from the calculated depth of the *sp* band in Fig. 4 plus the work function of 5.4 eV.

[19]P. S. Feibelman and D. E. Eastman, Phys. Rev. B **10**, 4932 (1974).

[20]P. J. Feibelman, Phys. Rev. B **26**, 5347 (1982).